Implications from GW170817 for Δ-isobar Admixed Hypernuclear Compact Stars

Jia Jie Li[1] and Armen Sedrakian[2,3]

[1] Institute for Theoretical Physics, J.W. Goethe University, D-60438 Frankfurt am Main, Germany; jiajieli@itp.uni-frankfurt.de
[2] Frankfurt Institute for Advanced Studies, D-60438 Frankfurt am Main, Germany; sedrakian@fias.uni-frankfurt.de
[3] Institute of Theoretical Physics, University of Wroclaw, 50-204 Wroclaw, Poland

Abstract

The effects of Δ-isobars on the equation of state of dense matter and structure of compact stars (CSs) are explored within the covariant density functional theory and confronted with the data on tidal deformability (TD) extracted from the GW170817 event. We show that the presence of Δ-isobars substantially softens the tension between the predictions of the hypernuclear density functionals and the inference from the observations of relatively small radius and small TD of canonical-mass CSs. The TDs deduced from GW170817 are compatible with the existence of hypernuclear CSs containing an admixture of Δ-isobars. We thus argue that the GW170817 event is consistent with a merger of a binary CS system having both strangeness (hyperons) and Δ-isobars in the stellar core.

Key words: equation of state – gravitational waves – stars: neutron

1. Introduction

The first multimessenger observations of gravitational waves (GWs) from the binary neutron star (NS) merger event, GW170817, marks the start of a new era in astronomy and astrophysics (Abbott et al. 2017a, 2017b, 2017c). The significance of this and future similar events lies, in part, in the opportunity of gaining insight into the equation of state (EoS) and composition of dense matter (Abbott et al. 2017b, 2018, 2019; Bauswein et al. 2017; Margalit & Metzger 2017; Soares-Santos et al. 2017; Villar et al. 2017; Rezzolla et al. 2018; Ruiz et al. 2018). In particular, the tidal deformability (TD; or polarizability) of NSs deduced from GW170817 puts already additional constraints on stellar radii and ultimately on the details of the EoS (Annala et al. 2018; De et al. 2018; Fattoyev et al. 2018; Most et al. 2018; Paschalidis et al. 2018; Tews et al. 2018; Zhang et al. 2018).

The potential implications of the GW170817 event cover a wide range of fundamental questions associated with NSs, ranging from their interior composition to their role in nucleosynthesis. In fact, a number of works have explored the possibility of using the observations of GW170817 to probe the occurrence of a hadron-quark phase transition (Blaschke & Chamel 2018; Burgio et al. 2018; Most et al. 2018; Paschalidis et al. 2018; Alvarez-Castillo et al. 2019).

Even at the level of the hadronic matter the composition of stellar matter could be rather complex. There have been intense studies of a number of possibilities of new degrees of freedom, such as hyperons (Glendenning 1985; Prakash et al. 1992; Weissenborn et al. 2012; van Dalen et al. 2014; Oertel et al. 2015; Tolos et al. 2016; Fortin et al. 2017; Li et al. 2018a), Δ-isobars (Prakash et al. 1992; Schürhoff et al. 2010; Drago et al. 2014; Cai et al. 2015; Kolomeitsev et al. 2017; Li et al. 2018b), or other exotic hadronic states such as $d^*(2380)$ resonance (Vidaña et al. 2018). The existence of hyperons inside NSs has been questioned for a long time because a class of models based on nonrelativistic microscopic treatments of dense matter were not able to produce massive enough ($M \sim 2 M_\odot$) stars. However, the hyperonization cannot be simply ruled out by the existence of $2 M_\odot$ stars. In particular, covariant density functional (CDF) based models are versatile enough to resolve the problem by tuning the interactions in the hyperonic sector

to hypernuclear data and compact star (CS) masses (Weissenborn et al. 2012; van Dalen et al. 2014; Oertel et al. 2015; Tolos et al. 2016; Fortin et al. 2017; Li et al. 2018a). Of course, one may also conjecture a layer of hypernuclear matter in between the nucleonic and quark matter phases (Bonanno & Sedrakian 2012; Masuda et al. 2013; Zdunik & Haensel 2013; Dexheimer et al. 2015). These models based on purely hyperonic EoSs predict CS sequences with $M_{max} \gtrsim 2.0 M_\odot$ and radii of the canonical-mass $M \sim 1.4 M_\odot$ star $R_{1.4} \gtrsim 13$ km (Katayama & Saito 2015; Fortin et al. 2016; Tolos et al. 2016; Li et al. 2018a; Li & Sedrakian 2019).

The possibility of hypernuclear stars with small radii ($R_{1.4} \lesssim 13$ km) is as exciting as it is challenging for nuclear theory. This requires a sufficiently soft EoS below 2–3 ρ_{sat}, where ρ_{sat} is the nuclear saturation density, while the observed large masses require that the same EoS must evolve into a stiff one at high densities. In this work, we construct such a model that is based on purely hadronic forms of stellar matter. We use the CDF theory (Meng et al. 2006) to explore the effects of the Δ-isobars on the TDs of CSs. We compare our results with the recent limits placed by the GW170817 event and discuss their implications for the interpretation and detection of the current and future GW signals from NS merger.

2. Tidal Deformability

Consider a static, spherically symmetric star, placed in a static external quadrupolar tidal field of the companion. As two stars approach each other during the early stages of an inspiral due to their mutual gravitational attraction they experience tidal deformation effects that can be quantified in terms of the TD λ. It can be expressed in terms of the dimensionless tidal Love number k_2 and the star's radius R as $\lambda = (2/3)k_2R^5$. The tidal Love number k_2 is calculated along with the solution of the Tolman–Oppenheimer–Volkov equations (Flanagan & Hinderer 2008; Hinderer 2008) and measures how easily the bulk of the matter in a CS is deformed (Flanagan & Hinderer 2008; Hinderer 2008; Binnington & Poisson 2009). It is more convenient to work with the dimensionless TD Λ, which is related to the Love number k_2 and the compactness parameter

$C = M/R$ through

$$\Lambda = \lambda/M^5 = \frac{2}{3}\frac{k_2}{C^5}. \qquad (1)$$

The total tidal effect of two CSs in an inspiraling binary system is given by the mass-weighted TD

$$\tilde{\Lambda} = \frac{16}{13}\left[\frac{(M_1 + 12M_2)M_1^4\Lambda_1}{(M_1 + M_2)^5} + 1 \leftrightarrow 2\right], \qquad (2)$$

where $\Lambda_1(M_1)$ and $\Lambda_2(M_2)$ are the TDs of the individual binary components. The quantity $\tilde{\Lambda}$ is usually evaluated as a function of the chirp mass $\mathcal{M} = (M_1 M_2)^{3/5}/M_T^{1/5}$ for various values of the mass ratio $q = M_2/M_1$, where $M_T = M_1 + M_2$ is the total mass of the binary.

3. Hadronic Matter EoS

Below we shall concentrate on the EoS of hypernuclear matter obtained from the CDF theory in its version that uses density-dependent meson–baryon couplings (Typel & Wolter 1999). The extension to the hyperonic sector is described elsewhere (Li et al. 2018a, 2018b), see also (Weissenborn et al. 2012; Fortin et al. 2017). A useful parameterization of the nucleonic EoS is given by the formula

$$E(\rho, \delta) \simeq E_{\text{sat}} + \frac{1}{2!}K_{\text{sat}}n^2 + \frac{1}{3!}Q_{\text{sat}}n^3 \\ + E_{\text{sym}}\delta^2 + L_{\text{sym}}\delta^2 n + \mathcal{O}\left(n^4, n^2\delta^2\right), \qquad (3)$$

where $n = (\rho - \rho_{\text{sat}})/3\rho_{\text{sat}}$ and $\delta = (\rho_{\text{n}} - \rho_{\text{p}})/\rho$. The coefficients entering the parameterization (3) are the nuclear characteristic parameters E_{sat} (binding energy), K_{sat} (compressibility), E_{sym} (symmetry energy), Q_{sat} (isoscalar skewness coefficient), and L_{sym} (isovector slope coefficient), all defined at ρ_{sat}. The low-order characteristics E_{sat}, K_{sat}, and E_{sym} are either strongly constrained or have no noticeable impact on the gross properties of CSs (Margueron et al. 2018; Li & Sedrakian 2019). Therefore, the remaining higher-order characteristic parameters are those that can be used to calibrate the parameters of the density functional to the desired properties of the system at hand (Li & Sedrakian 2019). Their values are weakly constrained by the conventional fitting protocol used in constructing the CDF. Specifically, their ranges can be constrained by χEFT computations of neutron matter (Drischler et al. 2016), and the requirement that the EoS reproduces the observed maximum mass of a CS $M_{\text{max}} \gtrsim 2\,M_\odot$ (Antoniadis et al. 2013). The low-order characteristic parameters for our models are the same as the values predicted by the DD-ME2 parameterization (Li et al. 2018b). The observations (Antoniadis et al. 2013) and recent inferences of M_{max} (Margalit & Metzger 2017; Rezzolla et al. 2018; Ruiz et al. 2018) enable one to limit the range of Q_{sat}. However, it should be stressed that such range will essentially depend on the composition of matter (Li & Sedrakian 2019). For instance, we have checked that the constraint $1.97 \lesssim M_{\text{max}}/M_\odot \lesssim 2.17$ limits Q_{sat} to the range $\sim[-650, -400]$ for purely nucleonic matter, and $\sim[300, 800]$ for hyperonic matter.

In Table 1 we present integral parameters of hyperonic CSs (maximum mass M_{max}, the radius $R_{1.4}$, and dimensionless TD $\Lambda_{1.4}$ of the canonical-mass star) for pairs of values of L_{sym} and

Q_{sat}. To obtain massive enough hypernuclear CSs, Q_{sat} values must be large (Li & Sedrakian 2019); as a result the radii for canonical stars obtained with these values of Q_{sat} are $R_{1.4} \gtrsim 13$ km (Katayama & Saito 2015; Fortin et al. 2016; Tolos et al. 2016; Li et al. 2018a; Li & Sedrakian 2019). The corresponding TDs are $\Lambda_{1.4} > 600$. To obtain smaller values of these parameters, which are favored by the observational data, we next explore the effect of Δ-isobars by varying the Δ-potential. The underlying EoS is parameterized in terms of the potential V_Δ of Δ-isobar in symmetric nuclear matter at ρ_{sat}.

To set the stage for the discussion of TDs of CSs in the next section we show in Figure 1 the mass–radius (MR) relations for purely nucleonic, hyperonic, and hyperon-Δ admixed stellar matter for a number of parameter values, as indicated in the figure. It is seen that the allowance of Δ-isobars in matter shifts the radii of configurations to smaller values without seriously affecting the value of the maximum mass ($M_{\text{max}} \gtrsim 2.0\,M_\odot$), an observation already made using alternative parameterizations of CDF in Drago et al. (2014) and Li et al. (2018b). We now turn to the discussion of our results for TDs.

4. Results and Discussions

The analysis of the GW170817 and complementary electromagnetic data could provide an important bound on the TDs. In particular, the LIGO/Virgo data analysis from GW170817 (hereafter LV constraint) placed an upper bound for the case of low-spin priors (Abbott et al. 2017b, 2019). We note that the LV detection of GW170817 derived an upper bound $\tilde{\Lambda} \lesssim 900$ (Abbott et al. 2017b) from the phase-shift analysis of the observed signal, and was recently reanalyzed to be $\tilde{\Lambda} \lesssim 720$ (Abbott et al. 2019). However, as this boundary is somewhat dependent on the waveform models, we use here all the data reported in Abbott et al. (2017b, 2019). A lower bound of $\tilde{\Lambda} \gtrsim 400$ is imposed by combining optical/infrared and GW data with new numerical relativity results (Radice et al. 2018). More recently, an alternative approach involving radiative transfer simulations for the electromagnetic transient AT 2017gfo predicts the lower bound to be $\tilde{\Lambda} \gtrsim 197$ (Coughlin et al. 2018). In the equal-mass scenario, these limits translate to constraints on the TD of a single CS itself.

In Figure 2 we show the tidal Love number k_2, the polarizability λ, and the dimensionless TD Λ of a CS as a function of its mass M. It is seen that the value of k_2 peaks for stellar configurations with mass near $0.8\,M_\odot$, while it decreases rapidly for both higher and lower mass configurations. The behavior of k_2 as a function of M as seen in Figures 2(a), (b) can be understood by noting that the more centrally condensed stellar models have smaller k_2 values (Hinderer et al. 2010).

The TD λ for the same set of EoSs is shown in Figures 2(c), (d). This parameter has a direct astrophysical significance because it is proportional to a quantity directly measurable by GW observations of inspiraling star binaries. As can be seen from Figures 2(c), (d), for each EoS λ follows a trend that is very similar to that of k_2. However, λ is, in addition, proportional to R^5 and thus it shows a more pronounced variation compared to k_2. The error bars that are shown in Figures 2(c), (d) denote the range of probable values of the TD λ for a star with $M = 1.362\,M_\odot$. The relatively small λ suggested by GW170817 implies that both the isoscalar and the isovector sectors of the EoS up to 2–$3\rho_{\text{sat}}$ should be soft. This, in turn, provides additional constraints for the nuclear characteristic parameters, in particular, the combinations of

Table 1
Properties of CSs Assuming Purely Hyperonic (Y) and Hyperon-Δ Admixed (Δ) Composition for Selected EoS Models

DF	Q_{sat}	L_{sym}	$M_{max}^{(Y)}$	$R_{1.4}^{(Y)}$	$\Lambda_{1.4}^{(Y)}$	$M_{max}^{(\Delta)}$	$R_{1.4}^{(\Delta)}$	$\lambda_{1.4}^{(\Delta)}$	$\Lambda_{1.4}^{(\Delta)}$
1	480	40	2.02	13.06	636	2.03–2.06	12.91–12.08	3.25–1.97	575–348
2	480	60	2.00	13.35	754	2.01–2.04	13.24–12.38	3.97–2.42	701–426
3	300	50	1.97	13.10	655	1.98–2.01	12.94–12.07	3.30–1.94	584–342
4	800	50	2.06	13.31	772	2.07–2.10	13.22–12.39	4.08–2.56	722–454

Note. The first three columns identify the EoS by the isoscalar skewness Q_{sat} (MeV) and isovector slope L_{sym} (MeV). The remaining columns display: maximum mass M_{max} ($M_\odot$), radius $R_{1.4}$ (km), TDs $\lambda_{1.4}$ (10^{36} gr cm^2 s^2), and $\Lambda_{1.4}$ of the canonical-mass CS. The results for hyperon-Δ admixed matter are obtained by tuning the Δ-potential V_Δ/V_N from 1 to 5/3.
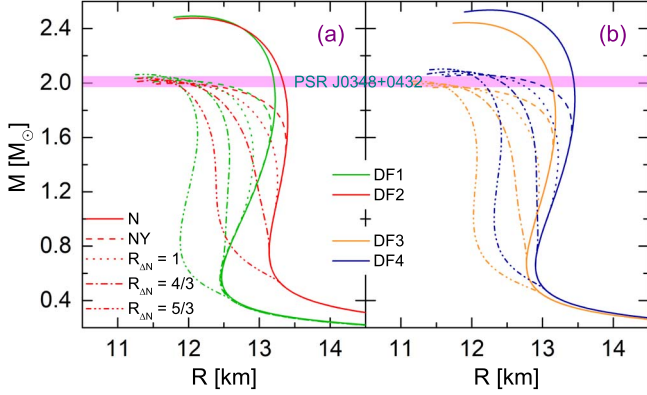

Figure 1. Mass–radius relation for a set of EoSs with varying L_{sym} (a) and Q_{sat} (b) and assuming purely nucleonic (N), hyperonic (NY), and hyperon-Δ admixed ($NY\Delta$) compositions of stellar matter. Three values of the Δ-potential have been used: $R_{\Delta N} = V_\Delta/V_N = 1$, 4/3, and 5/3, where V_N is the nucleon potential in isospin-symmetrical matter at saturation density.

Q_{sat} and L_{sym}. The dimensionless TD Λ for selected EoS models is presented in Figures 2(e), (f).

We now explore how the variations of Q_{sat} and L_{sym} affect the TDs of CSs. We concentrate only on the hyperonic models, but the conclusions also apply for Δ-admixed models. It is seen from Figures 2(c), (d) that the variation of L_{sym} from 40 to 60 MeV (with Q_{sat} fixed) as allowed by the χEFT calculations has appreciable effect on λ for less massive stars ($M \lesssim 1.4\,M_\odot$), whereas the variation of Q_{sat} from 300 to 800 MeV (with L_{sym} fixed) as allowed by both the χEFT and the maximum mass constraints has a more significant effect on λ of heavier stars ($M \gtrsim 1.4\,M_\odot$). The former observations on L_{sym} is consistent with previous studies (Fattoyev et al. 2013). Here we report, for the first time, a broad analysis of the effects of variations of Q_{sat}. The stars of interest ($M \approx 1.1$–$1.6\,M_\odot$) are just at the intersection where the effects of Q_{sat} and L_{sym} on the TD are comparable. Therefore, Q_{sat} or L_{sym} values alone are insufficient to characterize the low-density (up to $\sim2\rho_{sat}$) behavior of an EoS (Li & Sedrakian 2019). Further observations for binary merger events with smaller chirp mass will allow one to narrow down the uncertainty in L_{sym} (important for low-mass stars); larger chirp mass observations will constrain Q_{sat} more tightly (important for high-mass stars).

Below we discuss results for a single set of EoS models with fixed Q_{sat} and L_{sym}, but the conclusions also apply for other sets of models specified by these parameters. As already seen from the MR relation, accounting for Δ-isobars reduces the radii of models from their values obtained for purely hyperonic (or nucleonic) EoSs. As expected, the deeper the potential V_Δ, the larger the observed shift in the radius is and, accordingly, the larger the reduction of the TD. For example, for
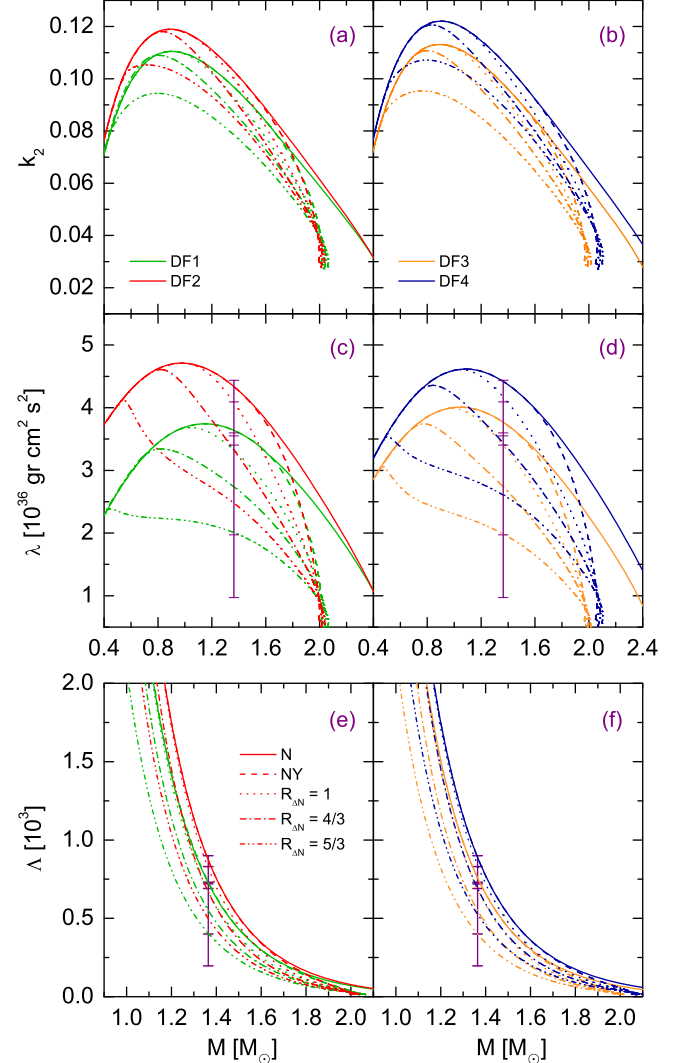

Figure 2. Tidal Love number k_2 (top), polarizability λ (middle), and dimensionless TD Λ (bottom) of a CS as a function of mass M for a set of EoSs with varying values of L_{sym} ((a), (c), (e)), Q_{sat} ((b), (d), (f)), and the Δ-potential. The error bars indicate the constraints on $\Lambda(\lambda)$ for an $M = 1.362\,M_\odot$ star, as estimated from the GW170817 event (Abbott et al. 2017b, 2019; Coughlin et al. 2018; Radice et al. 2018).

$V_\Delta/V_N = 5/3$ the radius of a canonical $1.4\,M_\odot$ CS is about 1 km smaller than the radius of its purely hyperonic (or nucleonic) counterpart. Correspondingly, the dimensionless TD of a canonical $1.4\,M_\odot$ CS is about 300 smaller than the value of its purely hyperonic counterpart; see Figures 2(e), (f).

Table 1 shows how the properties of CS (including the maximum mass, radius, and TD for a $1.4\,M_\odot$ star) change with
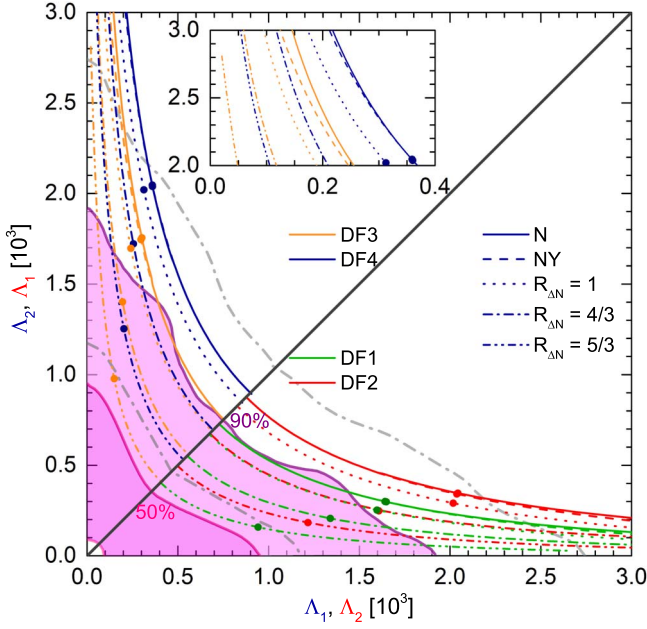
Figure 3. Dimensionless TDs associated with the binary in GW170817, predicted by a range of EoSs that allows various $L_{\rm sym}$ or $Q_{\rm sat}$ individually, and the Δ-potential. The shadings correspond to the updated 50% and 90% credibility regions (PhenomPNRT model) from the LV analysis (Abbott et al. 2019). The gray dashed–dotted curves represent the previously reported data (TaylorF2 model; Abbott et al. 2017b). The circles represent model predictions for a binary system having mass ratio $q = 0.73$.
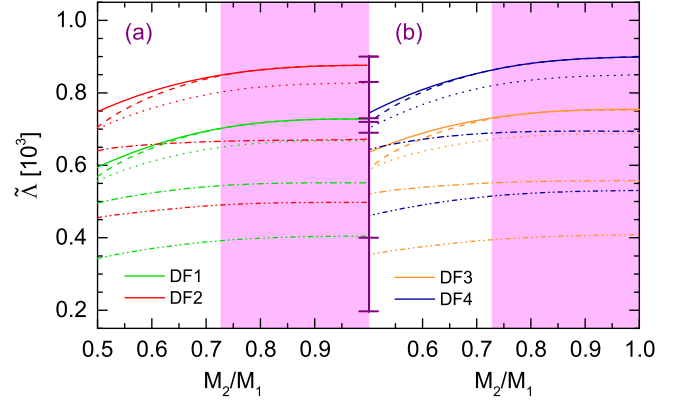

Figure 4. Mass-weighted TDs of the binary as a function of the mass ratio, assuming a chirp mass of $\mathcal{M} = 1.186 M_\odot$. The error bars indicate the constraints estimated from the GW170817 event (Abbott et al. 2017b, 2019) and the electromagnetic transient AT 2017gfo (Coughlin et al. 2018; Radice et al. 2018). The shadings show the mass ratio of the binary with 90% confidence, $q \gtrsim 0.73$ (Coughlin et al. 2018; Abbott et al. 2019).

the value of the Δ-potential V_Δ. The differences in the values of $\Lambda_{1.4}$ can be mapped on the differences in the compactness using the scaling $\Lambda \propto C^{-6}$ valid for moderate-mass stars (Hinderer et al. 2010; Postnikov et al. 2010). This scaling follows from the proportionality $k_2 \propto C^{-1}$, which is observed for a wide variety of EoSs in the mass range $1.1 \lesssim M/M_\odot \lesssim 1.6$ relevant for GW170817. This mass range corresponds roughly to $0.11 \lesssim C \lesssim 0.20$ (Hinderer et al. 2010; Postnikov et al. 2010). We note that for the same mass stars (e.g., $M = 1.4 M_\odot$) the larger the Δ-potential is the smaller the radii are and, therefore, the larger the compactness and the smaller the value of Λ.

We also observe in Figures 2(c), (d) that the mass corresponding to the maximum value of λ becomes smaller for EoS models that have a deeper potential V_Δ. As the increase in the maximum masses of CSs due to Δ-isobars is marginal, it, more importantly, affects medium-mass stars. For large enough Δ-potentials the isobars may appear already at about $2\rho_{\rm sat}$, which implies that even low-mass CSs can be affected by the populations of Δ-isobars; see Figures 2(c), (d). It is worth noticing that the reduction of TD caused by the inclusion of Δ-isobars in the composition of matter is not very sensitive to the exact values of $Q_{\rm sat}$ and $L_{\rm sym}$. However, the onset density of Δ-isobars and their fraction in the matter are sensitive to the values of $Q_{\rm sat}$ and $L_{\rm sym}$.

We now directly compare our modeling with the observational analysis from the GW170817 event, assuming a chirp mass $\mathcal{M} = 1.186 M_\odot$. We only investigate the more realistic low-spin case, because large spins are not expected from the observed galactic binary NS population (Abbott et al. 2018).

In Figure 3 we display predictions from all EoS models for the individual tidal polarizabilities Λ_1–Λ_2 associated with the M_1–M_2 components of the binary. The diagonal line corresponds to the case of an equal-mass binary, i.e.,

$M_1 = M_2 = 1.362 M_\odot$. The shaded areas correspond to the 90% and 50% confidence limits, which are obtained from the improved analysis of the GW170817 event (Abbott et al. 2019). The previously reported data (Abbott et al. 2017b) are also shown as they have been widely used to constrain EoS models.

It is clearly seen from Figure 3 that all the hyperonic (or nucleonic) EoS models satisfy the original 90% confidence (Abbott et al. 2017b), whereas the two sets of hyperonic EoS models, $(Q_{\rm sat}, L_{\rm sym}) = (800, 50)$ and $(480, 60)$ [MeV], are ruled out by the updated data (Abbott et al. 2019). The remaining two sets of hyperonic EoS models with $(Q_{\rm sat}, L_{\rm sym}) = (300, 50)$ and $(480, 40)$ [MeV] closely follow the updated 90% confidence (Abbott et al. 2019). As soon as the Δ-isobars appear in matter with reasonably attractive Δ-potential in nuclear matter $(V_\Delta < V_N)$ all EoS models are completely inside the region of compatibility with the data from GW170817. Thus, if the binary in the GW170817 event contained hadronic stars, the updated analysis would strongly favor the presence of Δ-isobars in addition to hypernuclear matter, as our purely hyperonic EoS models are rather representative of this class of models. An alternative is the strong phase transition to a quark matter phase, as it has been shown that such a transition also helps in producing more compact objects than those composed of nucleons only (Kojo et al. 2016; Alford & Sedrakian 2017; Blaschke & Chamel 2018; Montana et al. 2018; Alvarez-Castillo et al. 2019; Xia et al. 2019).

Interestingly, the Λ_1–Λ_2 curves predicted by EoS models in the parameter spaces $(Q_{\rm sat}, L_{\rm sym}, V_\Delta) = (480, 40, V_N)$ and $(480, 60, 4/3V_N)$ MeV are almost identical, but their MR relations are noticeably different. This is because the two MR curves cross around $M = 1.4 M_\odot$ and converge to each other at $M \simeq 2.0 M_\odot$; see Figure 1(a). It is thus possible that different M_1–M_2 components of the binary have almost the same polarizabilities Λ_1–Λ_2.

For the sake of completeness, in Figure 4 we show the mass-weighted average TD $\tilde{\Lambda}$ with the ratio of masses of merger components for a fixed chirp mass $\mathcal{M} = 1.186 M_\odot$. It is seen that $\tilde{\Lambda}$ depends weakly on the mass ratio q. The boundaries on $\tilde{\Lambda}$, which were set by the GW and electromagnetic spectrum observations, respectively, are also shown. We should mention

that the estimates of both boundaries are strongly model dependent (Abbott et al. 2017c, 2019; Coughlin et al. 2018; Most et al. 2018; Radice et al. 2018), especially the lower limit. The lower limit calculated from the Δ-isobar featuring EoS models is about 350. Further reduction of the radius by up to 2 km can be obtained for larger values of V_Δ; see Li et al. (2018b) for a detailed discussion. In turn, $\tilde{\Lambda}$ could be decreased in this case.

5. Summary

In this work, we have explored the TDs of CSs featuring hypernuclear matter with an admixture of Δ-isobars. As a consequence of including Δ-isobar degrees of freedom, the dimensionless TD $\Lambda_{1.4}$ for canonical-mass stars is reduced by about 300 for reasonably attractive Δ-potential. Thus, the presence of Δ-isobars lifts the tension between the predictions of the hypernuclear density functionals (which predict large TD) and the observations, which imply small TD.

In addition, we found that the nuclear characteristics Q_{sat} and L_{sym} control the TDs of large- and small-mass stars, respectively, whereas they are equally important for the TDs of canonical mass $M \simeq 1.4\,M_\odot$ stars. Thus, one may conclude that the GW170817 event is highly useful in constraining these universal parameters.

ORCID iDs

Jia Jie Li (ORCID) https://orcid.org/0000-0001-8635-3939
Armen Sedrakian (ORCID) https://orcid.org/0000-0001-9626-2643

References

Abbott, B. P., Abbott, R., Abbott, T. D., et al. 2017a, ApJL, 848, L13
Abbott, B. P., Abbott, R., Abbott, T. D., et al. 2017b, PhRvL, 119, 161101
Abbott, B. P., Abbott, R., Abbott, T. D., et al. 2018, PhRvL, 121, 161101
Abbott, B. P., Abbott, R., Abbott, T. D., et al. 2019, PhRvX, 9, 011001
Abbott, B. P., Abbott, R., Adhikari, R. X., et al. 2017c, ApJL, 848, L12
Alford, M., & Sedrakian, A. 2017, PhRvL, 119, 161104
Alvarez-Castillo, D. E., Blaschke, D. B., Grunfeld, A. G., & Pagura, V. P. 2019, PhRvD, 99, 063010
Annala, E., Gorda, T., Kurkela, A., & Vuorinen, A. 2018, PhRvL, 120, 172703
Antoniadis, J., Freire, P. C. C., Wex, N., et al. 2013, Sci, 340, 6131
Bauswein, A., Just, O., Janka, H.-T., & Stergioulas, N. 2017, ApJL, 850, L34
Binnington, T., & Poisson, E. 2009, PhRvD, 80, 084018
Blaschke, D., & Chamel, N. 2018, ASSL, 457, 337
Bonanno, L., & Sedrakian, A. 2012, A&A, 539, A16
Burgio, G. F., Drago, A., Pagliara, G., Schulze, H.-J., & Wei, J.-B. 2018, ApJ, 860, 139
Cai, B.-J., Fattoyev, F. J., Li, B.-A., & Newton, W. G. 2015, PhRvC, 92, 015802
Coughlin, M. W., Dietrich, T., Doctor, Z., et al. 2018, MNRAS, 480, 3871
De, S., Finstad, D., Lattimer, J. M., et al. 2018, PhRvL, 121, 091102
Dexheimer, V., Negreiros, R., & Schramm, S. 2015, PhRvC, 91, 055808
Drago, A., Lavagno, A., Pagliara, G., & Pigato, D. 2014, PhRvC, 90, 065809
Drischler, C., Carbone, A., Hebeler, K., & Schwenk, A. 2016, PhRvC, 94, 054307
Fattoyev, F. J., Carvajal, J., Newton, W. G., & Li, B.-A. 2013, PhRvC, 87, 015806
Fattoyev, F. J., Piekarewicz, J., & Horowitz, C. J. 2018, PhRvL, 120, 172702
Flanagan, E. E., & Hinderer, T. 2008, PhRvD, 77, 021502
Fortin, M., Avancini, S. S., Providência, C., & Vidaña, I. 2017, PhRvC, 95, 065803
Fortin, M., Providência, C., Raduta, A. R., et al. 2016, PhRvC, 94, 035804
Glendenning, N. K. 1985, ApJ, 293, 470
Hinderer, T. 2008, ApJ, 677, 1216
Hinderer, T., Lackey, B. D., Lang, R. N., & Read, J. S. 2010, PhRvD, 81, 123016
Katayama, T., & Saito, K. 2015, PhLB, 747, 43
Kojo, T., Powell, P. D., Song, Y., & Baym, G. 2016, NuPhA, 956, 821
Kolomeitsev, E. E., Maslov, K. A., & Voskresensky, D. N. 2017, NuPhA, 961, 106
Li, J. J., Long, W. H., & Sedrakian, A. 2018a, EPJA, 54, 133
Li, J. J., & Sedrakian, A. 2019, arXiv:1903.06057
Li, J. J., Sedrakian, A., & Weber, F. 2018b, PhLB, 783, 234
Margalit, B., & Metzger, B. D. 2017, ApJL, 850, L19
Margueron, J., Hoffmann Casali, R., & Gulminelli, F. 2018, PhRvC, 97, 025806
Masuda, K., Hatsuda, T., & Takatsuka, T. 2013, ApJ, 764, 12
Meng, J., Toki, H., Zhou, S.-G., et al. 2006, PPNuPh, 57, 470
Montana, G., Tolos, L., Hanauske, M., & Rezzolla, L. 2018, arXiv:1811.10929
Most, E. R., Weih, L. R., Rezzolla, L., & Schaffner-Bielich, J. 2018, PhRvL, 120, 261103
Oertel, M., Providência, C., Gulminelli, F., & Raduta, A. R. 2015, JPhG, 42, 075202
Paschalidis, V., Yagi, K., Alvarez-Castillo, D., Blaschke, D. B., & Sedrakian, A. 2018, PhRvD, 97, 084038
Postnikov, S., Prakash, M., & Lattimer, J. M. 2010, PhRvD, 82, 024016
Prakash, M., Prakash, M., Lattimer, J. M., & Pethick, C. J. 1992, ApJL, 390, L77
Radice, D., Perego, A., Zappa, F., & Bernuzzi, S. 2018, ApJL, 852, L29
Rezzolla, L., Most, E. R., & Weih, L. R. 2018, ApJL, 852, L25
Ruiz, M., Shapiro, S. L., & Tsokaros, A. 2018, PhRv, 97, 021501
Schürhoff, T., Schramm, S., & Dexheimer, V. 2010, ApJL, 724, L74
Soares-Santos, M., Holz, D. E., Annis, J., et al. 2017, ApJL, 848, L16
Tews, I., Margueron, J., & Reddy, S. 2018, PhRvC, 98, 045804
Tolos, L., Centelles, M., & Ramos, A. 2016, ApJ, 834, 3
Typel, S., & Wolter, H. H. 1999, NuPhA, 656, 331
van Dalen, E., Colucci, G., & Sedrakian, A. 2014, PhLB, 734, 383
Vidaña, I., Bashkanov, M., Watts, D. P., & Pastore, A. 2018, PhLB, 781, 112
Villar, V. A., Guillochon, J., Berger, E., et al. 2017, ApJL, 851, L21
Weissenborn, S., Chatterjee, D., & Schaffner-Bielich, J. 2012, PhRvC, 85, 065802
Xia, C.-J., Maruyama, T., Yasutake, N., & Tatsumi, T. 2019, arXiv:1902.08766
Zdunik, J. L., & Haensel, P. 2013, A&A, 551, A61
Zhang, N.-B., Li, B.-A., & Xu, J. 2018, ApJ, 859, 90